Single-track length measurements of step-etched fission tracks in Durango apatite: *Vorsprung durch Technik*

RAYMOND JONCKHEERE*, MURAT T. TAMER†, FLORENTINE WAUSCHKUHN, BASTIAN WAUSCHKUHN AND LOTHAR RATSCHBACHER

Geologie, Technische Universität Bergakademie Freiberg, 09599 Freiberg (Sachsen), Germany

ABSTRACT

Fossil and induced confined fission tracks in Durango apatite do not etch to their full etchable lengths with the current protocols. Their mean lengths continue to increase at a diminished rate past the break in slope in a length *versus* etch-time plot, from whereon they are considered to be fully etched. The mean length of the fossil tracks increases from 14.5(1) to 16.2(1) µm and that of the induced tracks from 15.7(1) to 17.9(1) µm between 20s and 60s etching (5.5 M HNO_3; 21 °C); both are projected to converge towards ~18 µm after ~180 s. This increase is due to track etching, not simple bulk etching. The irregular length increments of individual tracks reveal a discontinuous track structure in the investigated length intervals. The mean lengths of the fossil and induced tracks for the standard etch time (20 s) for the (5.5 M HNO_3; 21 °C) etch are thus not the result of a simple shortening of the latent fission tracks but instead of a lowering of the effective track-etch rate v_T. The rate of length increase of individual fossil confined tracks correlates with their length: older tracks are shorter because they etch more slowly. Step etching thus makes it possible to some extent to distinguish between older and younger fossil fission tracks. Along-track v_T measurements could reveal further useful paleo-temperature information. Because the etched length of a track at standard etch conditions is not its full etchable length, geometrical statistics based on continuous line segments of fixed length are less secure than hitherto held.

KEYWORDS

Durango apatite; fission track; step etching; confined-track length

* Corresponding author: Raymond.Jonckheere@geo.tu-freiberg.de
† Present address: Jackson School of Geosciences, The University of Texas at Austin, Austin, Texas, U.S.A.

BACKGROUND

The conventional fission-track method distinguishes itself from other radiometric geothermochronometers in that both the parent- and daughter-isotope concentrations are measured by means of proxies. The fossil tracks stand for the daughters produced by spontaneous nuclear fission of ^{238}U. The induced tracks created by thermal-neutron fission of ^{235}U stand for the present concentration of the parent. The damage trails left in the wake of the fission fragments' flight have dimensions (length: ~21 μm; Bhandari et al., 1971; Jonckheere, 2003; diameter: <10 nm; Paul and Fitzgerald, 1992) and structure (Miro et al., 2005; Afra et al., 2011; Li et al., 2014; Schauries et al., 2014; Lang et al., 2015). Latent fission tracks are thus susceptible to changes effected by environmental factors, with temperature as the main factor (Fleischer et al., 1964, 1974, 1975; Kohn et al., 2003; Schmidt et al., 2014). Each fossil track holds a record of the temperature effects it experienced from its formation to the present. Apatite fission-track modeling was developed to exploit this stored information for reconstructing the thermal histories of geological samples.

The temperature record stored in the fossil tracks is read from the length distribution of etched confined tracks. Etching condenses the information in individual tracks into a single scalar value: their etchable length. Tracks that experienced the same environmental conditions are however not all etched to the same length as a result of random factors involved in uranium fission, track formation, and repair. Their temperature information is therefore reflected in the mean of their etched-length distribution. Length variations due to the possible effects of the anisotropic properties of the track detector on track formation, annealing, and etching are systematic and can be accounted for (Galbraith and Laslett, 1988; Donelick, 1991; Donelick et al., 1999; Galbraith, 2002; Ketcham et al., 2007).

Step-etch experiments show that the mean length of induced fission tracks in apatite increases fast up to an etch strength S_E (S_E = etchant concentration (M) × etch time (s)) of ~50 M.s, followed by a slow - or no - increase (Figure 1). The data scatter prevents us from concluding whether the transition is gradual or not. Etching to just past the transition point ($60 \lesssim S_E \lesssim 90$) is considered ideal; tracks on either side are either "under-etched" or "over-etched" (Laslett et al., 1984). The basic model holds that the confined-track length increases at twice the track-etch rate v_T until the etchant reaches both ends, and the track is revealed over its full etchable length, and at twice the bulk-etch rate v_B thereafter (Laslett et al., 1984). The lack of experimental evidence of bulk etching (Figure 1; except f) was explained by the fact that most of the measured tracks at each etch step represent a new sample of confined tracks (Green et al., 1986). Both the

Barbarand et al. (2003) data for under-etched tracks (S_E < 60 M.s; Figure 1j) and the Carlson et al. (1999) data for over-etched tracks (S_E > 90 M.s; Figure 1f) lie above the fitted trend. This could be due to a stricter selection of well-etched tracks for length measurement, compared to the other experiments. This could itself be a bias resulting from the attempt to measure underetched tracks or from the use of Cf-irradiation for increasing the number of measureable confined tracks close to the sample surface, or from other causes.

It is important to distinguish etch effects from temperature effects for extracting temperature data from length measurements of etched fossil confined tracks. This contribution reports the results of a step-etch experiment aimed at a better understanding of track etching. It exploits the advantages of software-controlled motorized microscope stages for recording the position of each confined track and revisiting it after each succeeding step, enabling the investigation of the same track population after each step and the re-measurement of individual track lengths rather than the population mean. In this manner, we compare fossil and induced fission tracks, in annealed and un-annealed Durango apatite. This allows us to address two important questions: "do fossil tracks etch like induced tracks?", and "do induced tracks in a natural apatite etch as in annealed apatite?".

EXPERIMENT

We cut three ~1 mm-thick sections parallel to the ***c***-axes of cm-sized Durango apatite crystals with a Struers Accutom-50 precision saw. We annealed one section for 24 h at 450 °C in a Gero tube furnace to erase the fossil tracks and exposed it together with an un-annealed section to a nominal thermal-neutron fluence of 5×10^{15} cm^{-2} in channel X26 of the BR-1 reactor (SCK•CEN Mol, Belgium) to produce induced fission tracks. We neither annealed nor irradiated the third section, which retained its natural complement of fossil fission tracks. We mounted the three sections in Araldite resin, ground them with #1200 SiC sanding paper, and polished the exposed surfaces with 6-, 3-, and 1-µm diamond suspensions on a Struers RotoPol-35 apparatus equipped with a PdM-Force-20 sample holder. After polishing, we reduced the mount thicknesses to ~2 mm and affixed them to microscope slides. We etched the tracks in 5.5 M HNO_3 at 21.0 ± 0.1 °C for 20 s (Carlson et al., 1999), and rinsed them immediately upon extraction from the solution successively in two large volumes of fresh deionised water in order to arrest etching. We measured the confined-track lengths with a Zeiss M2m microscope with a motorized stage connected to a desktop computer running the Zeiss AxioVision software, which permits recording the coordinates, length and orientation of each track. We then re-etched the samples for 10 s under the same conditions as before, and re-measured each confined track, except those that we could not measure again, because their ends were hidden by neighboring tracks or because they had been exhumed due to bulk etching of the apatite surface. We repeated this procedure three more times, giving five length measurements for each surviving track. All measured tracks were included in the statistics up to the point that they were lost. Tables 1 and 2 summarize the length data.

RESULTS AND DISCUSSION

Confined-track lengths

Figures 2 and 3 show the track-length distributions and scatter plots of the track lengths against their angles to the ***c***-axis. The results of the 20-s etch are consistent with published data. The mean length of the induced tracks (15.67(06) μm) agrees within statistical error with the overall mean for several laboratories using different etch conditions (15.89(12) μm; Ketcham et al., 2015). The mean length of the fossil tracks (14.47(05) μm) agrees with the mean for different etches listed in Jonckheere et al. (2015, Table 2; 14.35(08) μm). The mean for the sample with both fossil and induced tracks (15.63(08) μm) is intermediate between these values but close to that of the induced tracks. This is consistent with the nominal neutron fluence (5×10^{15} cm^{-2}), corresponding to a ratio of volumetric latent track densities $N_S/N_I = 0.12$ (~11% fossil (N_S) and ~89% induced (N_I) tracks)[1].

Gaussian functions provide a good fit to the fossil- and induced-track-length distributions and even to the length distribution of the sample with both fossil and induced tracks (Table 1; Figure 2); this is an observation. The length distribution of the fossil tracks is the mean-length-weighted sum of those tracks that underwent different geological length shortening; that of the sample with fossil and induced tracks also includes tracks that experienced no geological length reduction. There is also no physical imperative for a Gaussian distribution of the induced-track lengths. The fits are therefore considered coincidental. The means and standard deviations of the fitted Gaussian distributions are nevertheless in agreement with the corresponding statistics based on the raw data (Table 1). The standard deviations of the fossil- (0.86 μm) and induced-track-length distributions (0.93 μm) are consistent with predictions based on the mean

[1] The purpose of the sample with fossil and induced tracks is to compare the etching of induced tracks in natural and annealed apatite. The neutron fluence was calculated to swamp the sample with induced tracks while keeping the track density low enough for track-length measurements at extended etch times. We observed, however, that the track statistics are almost exactly those of a weighted sum of the fossil and induced tracks, and analysed the results accordingly.

track lengths (Carlson et al., 1999; Donelick et al., 1999; Ketcham et al., 2000; Ketcham, 2005). Ellipses fitted to the length-*versus*-orientation data are in broad agreement with model expectations (Figure 3) but indicate somewhat less anisotropic track lengths than earlier studies using the same etchant (Donelick, 1991; Donelick et al., 1999; Ketcham, 2003); induced tracks: L_A/L_C = 1.00(01); fossil tracks: L_A/L_C = 0.94(01); L_A = minor axis; L_C = major axis). The minor and major axes of an ellipse fitted to the sample with both fossil and induced tracks are in numerical agreement with the fraction-weighted and length-bias-corrected values calculated from the corresponding axes of the ellipses fitted to the fossil- and induced-track data.

The track-length distributions retain an approximate Gaussian shape through consecutive etch steps (Figure 2) with little change of their standard deviations but a clear increase of their means (Table 1). Figure 4 shows the means, standard deviations and ***c***- and ***a***-axis lengths plotted against etch time. The mean length of the induced tracks increases at a somewhat different rate than that of the fossil tracks (Figure 4a). Both rates drop off with increasing etch time but the decrease of that of the induced tracks is more marked than that of the fossil tracks. The mean confined-track length and its rate of increase of the sample with both fossil and induced tracks are intermediate between the two and consistent with the fraction-weighted and length-bias-corrected average of the values for the fossil and induced fission tracks. The extrapolated mean track lengths of the three samples converge on ~18 μm at ~180 s etch time. This could indicate that fossil and induced tracks have the same maximum etchable length, ~20% shorter than the combined range of the fission fragments (21.9(9) μm; Jonckheere, 2003), or it could be a coincidence. The standard deviations of the length distributions of fossil and induced tracks also exhibit a different dependence on etch time (Figure 4b). That of the fossil tracks increases, while that of the induced tracks passes through a minimum at 40 s. That of the fossil plus induced tracks remains high despite a small decrease.

An elliptical model continues to provide an acceptable description of the variation of track length with orientation at longer etch times (30-60 s; Table 1; Figure 3). Both the fossil- and induced-track lengths become more anisotropic (Figure 4c). The trends are weak but nevertheless systematic and that of the fossil tracks is somewhat more pronounced than that of the induced tracks. The trend for the sample with fossil and induced tracks is intermediate between the two, and the ***c***- and ***a***-axis lengths of the fitted ellipses are consistent with the fraction-weighted and length-bias-corrected averages of the ***c***- and ***a***-axis lengths of the samples with fossil and induced fission tracks (Tables 1 and 2).

Track-length increments

Figure 5 shows the distributions of the length increments between consecutive etch steps and Figure 6 scatter plots of the increments *versus* the track angles to the ***c***-axis. The increments are not constant but irregular. Most are <1 μm but some up to 2 μm and even 3 μm. The distributions of the length increments are therefore skewed to the right in Figure 5. The average increment is more or less constant for the fossil tracks but decreases with each consecutive etch step for the induced fission tracks. The range of individual increments is also broadest from the first to the second step (20-30 s) and decreases thereafter, which is reflected in the standard deviations (Table 3). The first increment (20-30 s) is greater for both samples containing induced fission tracks than for that with only fossil tracks. The scatter plots show that the length increments do not correlate with the track orientations. The tracks lost after each step are also uncorrelated with their orientations.

A comparison of the lengths of individual tracks before and after each etch step (Figure 7) provides a means of examining the correlation between the track-length increments and track lengths. For the first step (20-30 s etching), the larger length increments are associated with the shorter tracks in both samples containing induced tracks but with the longer tracks in the sample with fossil tracks. The case of the induced tracks can be understood as a consequence of the operators' criteria for selecting well-etched tracks. The operators in this case judged some tracks well etched after 20 s that could after 30 s be reclassified as having been under-etched, based on their shorter starting lengths and larger increments. Such subjective decisions could have contributed to the large spread of mean induced-track lengths reported in a blind experiment (Ketcham et al., 2015). The fact that this is not the case for the fossil tracks seems to indicate that the length measurements of these tracks are less susceptible to judgement calls than are those of the induced tracks. It is not improbable that this is related to the smaller average increments.

The increase of the induced-track length through subsequent steps is less clear. The results for both samples with induced tracks provide no positive indication of a correlation with track length after 30 s. The weak anti-correlation between the initial (20 s) and final (60 s) lengths (Figure 8) can be attributed to the first increment (20-30 s; Figure 7). The statistics of the sample with fossil and induced tracks are consistent with the fraction-weighted and length-bias-corrected averages of the fossil and the induced tracks (Tables 1-3; Figures 4a, c). This signifies that the induced-track lengths and their rate of increase in the natural and annealed sample are the same. Low self-irradiation-damage densities ($D_\alpha \leq 10^{16}$ g^{-1} for ≤20 ppm U and ≤350 ppm Th, ignoring Sm; Young et al., 1969; Kimura et al., 2000; Boyce and Hodges, 2005; Morishita et al., 2008; Johnstone et al., 2013; Abdullin et al., 2014; Chew et al., 2014; Soares et al., 2014) thus appear to have no effect on the formation or immediate reorganization (Donelick et al., 1991) of fission tracks, at least none that is detectable by step etching. An earlier investigation reported identical track openings (D_{par}; Donelick, 1993; 1995; Burtner et al., 1994) of fossil and induced tracks in Durango apatite (etched 15-45 s in 4.0 M HNO_3 at 25 °C; Jonckheere et al., 2007). Both these observations suggest that neither self-irradiation damage nor that from neutron irradiation affect the bulk-etching properties of this apatite - or have the same effect.

The case of the fossil tracks wants a different explanation. We can exclude that the correlation between their initial length (20 s) and length increase is due to track-to-track differences resulting from variable uranium fission or random effects during track formation, because these also affect the induced tracks. The observed correlation must thus be related to the geological histories (ages) of individual fossil tracks. Single-track step-etch experiments thus enable us to distinguish between older shorter tracks with lower terminal etch rates (e.g., v_T = 2.0 µm/min for L_M = 13 µm) and younger longer tracks with higher terminal etch rates (e.g., v_T = 3.0 µm/min for L_M = 16 µm). It therefore appears possible that step-etch experiments might allow distinguishing successive generations of fossil tracks in geological samples and provide additional details about the environmental factors (temperatures) that affected them, resulting in more detailed thermal histories.

The length increase of both the fossil and induced tracks with increasing etch time is not the result of bulk etching (v_B) but of track etching (v_T). Simple bulk etching cannot account for the unequal length increases between steps or track-to-track differences. Simple bulk etching is also inconsistent with the diminishing rate of increase of the induced-track lengths and the different rates of increase of the fossil and induced track lengths. Radiation damage in the sample with fossil tracks is not the cause of the latter difference, since the induced tracks in the annealed and unannealed sample exhibit the same behavior. It follows that the fossil and induced tracks are longer than their measured lengths at the standard etch time (20 s). The fact that fossil tracks can be etched to lengths (16.21(08) µm; 60 s; Table 1) exceeding those of induced tracks at standard etch conditions (15.67(06) µm; 20 s) but appear shorter (14.47(05) µm; 20 s) is thus not the result of an actual shortening of the latent tracks but of a lowering of the effective track-etch rate v_T, at least in the investigated length intervals. The fact that induced tracks can be etched to 17.92(08) µm (60 s; Table 1) implies that a lowering of v_T also explains their length reduction in the time interval between 10-11 minutes (Durango: 16.6(1) µm; 25 s in 5 M HNO_3 at 23 °C; Donelick et al., 1991) and 41 days (16.2(1) µm) after the neutron irradiation that produced them.

Track structure

The irregular length increments of individual tracks past the break in slope favor a discontinuous (Dartyge et al., 1981; Pellas and Perron, 1984; Dartyge and Sigmund, 1985; Green et al. 1986; Paul and Fitzgerald, 1992; Hejl, 1995; Villa et al., 1999; Jaskierowicz et al., 2004; Li et al., 2011; 2012; 2014) over a continuous (Carlson, 1993; Afra et al., 2011; Kluth et al., 2012; Schauries et al., 2014) damage model. The high etch rate before the break in slope (40-50 μm/min) in the length *versus* etch-strength plot (Figure 1) suggests a more continuous central track section. Although it is evident that our observations are related to the earlier experiments of Green et al. (1986), there are also differences. Their gap model refers to tracks at high angles to the ***c***-axis near complete annealing, whereas our results refer to fossil and induced tracks with all orientations in samples that experienced nothing more than ambient-temperature annealing. Our observations also relate to terminal track sections that are not etched under standard conditions. Green et al. (1986) distinguished two stages in the annealing of fission tracks in apatite: a gradual shrinkage of the tracks resulting from gentle to moderate annealing, followed by the appearance of gaps on more severe annealing. This raises the question whether the gradual stage of Green et al. (1986) is in fact gradual at the level of individual tracks, or only at the level of their mean lengths. The mean lengths for our step-etch experiments also appear to increase in a gradual fashion.

The fact that the track sections from 14.5 to 16.2 μm (fossil tracks) and from 15.7 to 17.9 μm (induced tracks) can be etched also implies that their starting lengths, in general attributed to (ambient temperature) annealing, are not a result of an actual shortening of the latent tracks but of a lowering of the effective track-etch rate. The notion of a discontinuous track, made up of slower and faster etching sections, confounds the meaning of the track-etch rate. However, an effective etch rate v_T can be defined as the length of an etched section divided by the time it takes to etch; v_T averages over the length of the considered section and varies along the track. Because it is measured along the track and determined by the remains of the original track rather than the pre-existing lattice, we continue to refer to v_T as a track-etch rate. A lowering of v_T could result from a reorganization of faster- and slower-etching (gap) sections, or from a lowering of the etch rate of either, or both. Our observations nevertheless allow some tentative suppositions, although we need more experiments to confirm them. (1) The unequal increments from track to track suggest that the separation between successive gaps is of the order of substantial fractions of a micrometer rather than smaller, i.e. the track is discontinuous at a course scale. (2) The significant drop of the etch rate at the track ends compared to its midsection indicates that gaps exert a strong influence over the effective etch rate v_T. (3) In view of this, the fact that the induced tracks length increases at almost the same rate parallel and perpendicular to the c-axis, i.e. the lack of a pronounced anisotropy (Figure 4c), suggests that gaps etch at a higher rate than that of the pristine lattice, perhaps assisted by residual defects. (4) The slower and more anisotropic length increase of the fossil tracks could then both result from a depletion of residual defects in the gaps. (5) The remaining track segments and gaps nevertheless have contrasting etch rates.

The observation that there exist, under standard conditions, no full-length tracks, implies that the etched length of a track cannot be equated with its etchable length. The application of geometrical statistics based on continuous line segments of fixed length is thus problematic (Laslett et al., 1984). Considering that (1) otherwise unetchable terminal sections of surface-intersecting tracks can be etched by surface-assisted sub-threshold etching (Wauschkuhn et al., 2015b) and that (2) a limited shortening of fossil confined tracks does not cause a proportionate lowering of the fission-track age (Gleadow and Duddy, 1981; Gleadow et al., 1983; Wauschkuhn et al., 2015a; Jonckheere et al., 2015), the current model relating surface-track densities to mean confined-track lengths (Laslett et al., 1984; Galbraith and Laslett, 1988; Galbraith et al., 1990; Galbraith, 2002; Ketcham, 2003) is less secure than we assume. Jonckheere et al. (2015) calculated the effective lengths ($l_E = 2\rho/N$; ρ: surface-track density; N; volume-track density) of fossil and induced tracks in Durango apatite (fossil: 16.3(3) µm; induced: 16.8(4) µm). This bears out that surface tracks can etch to longer lengths than confined tracks by surface-assisted sub-threshold etching (Wauschkuhn et al., 2105b).

IMPLICATIONS

Computer-controlled motorized microscopes and software make it possible to perform repeated length measurements of individual confined fission tracks. The lengths of fossil and induced tracks in apatite continue to increase in fits and starts past the point where they are supposed to be well etched. This is due to etching of intermittent damage along the tracks, not to bulk etching. The application of geometrical statistics based on continuous line segments of fixed length is thus questionable. This implies that the theoretical relationship between surface-track densities and mean confined-track lengths must be re-examined. Other empirical relationships, such as that between the standard deviation and mean of the track-length distribution and that between the mean, ***a***-axis- and ***c***-axis-projected confined-track lengths remain valid under the conditions under which they were established, but should not be used with different etching conditions. The mean rate of length increase of individual fossil confined tracks is correlated with their length. Step etching thus makes it possible, to some extent, to distinguish between slower-etching older tracks and faster-etching younger tracks. Geological applications based on step-etching, e.g., involving two steps (20 s and 40 s), would have the advantage of tightening the distribution of the induced tracks and stretching that of the fossil tracks, which would in principle contribute to an increased resolution of the resulting temperature-time paths. Along-track etch-rate measurements could reveal additional paleo-temperature information. This needs a serious calibration effort but has the potential of realizing significant progress in apatite fission-track modeling.

Acknowledgement

Work supported by the German Research Foundation (DFG grants JO 358/3 and RA 442/27). We are obligated to B. Van Houdt (BR-1 reactor; SCK•CEN Mol, Belgium) for the thermal-neutron irradiation, and to P. Van den haute (Ghent University, Belgium) for discussion of the manuscript. We are indebted to E. Sobel (University of Potsdam) and an unnamed referee for their insightful comments.

References

Abdullin, F., Solé J., and Solari, L. (2014) Fission-track dating and LA-ICP-MS multi-elemental analysis of the fluorapatite from Cerro de Mercado (Durango, Mexico). Revista Mexicana de Ciencias Geológicas, 31, 395-406 (in Spanish).

Afra, B., Lang, M., Rodriguez, M., Zhang, D.J., Giulian, R., Kirby, N., Ewing, R.C., Trautmann, C., Toulemonde, M., and Kluth, P. (2011) Annealing kinetics of latent particle tracks in Durango apatite. Physical Review B, 83, 064116/1-5.

Barbarand, J., Hurford, A., and Carter, A. (2003) Variation in apatite fission-track length measurement: implications for thermal history modelling. Chemical Geology, 198, 77-106.

Boyce, J.W., and Hodges, K.V. (2005) U and Th zoning in Cerro de Mercado (Durango, Mexico) fluorapatite: insights regarding the impact of recoil redistribution of radiogenic 4He on (U-Th)/He thermochronology. Chemical Geology, 219, 261- 274.

Burtner, R.L., Nigrini, A., and Donelick, R.A. (1994) Thermochronology of lower Cretaceous source rocks in the Idaho-Wyoming Thrust Belt. American Association of Petroleum Geologists Bulletin, 78, 1613-1636.

Carlson, W.D. (1990) Mechanisms and kinetics of apatite fission-track annealing. American Mineralogist, 75, 1120-1139.

Carlson, W.D., Donelick, R.A., and Ketcham, R.A. (1999) Variability of apatite fission-track annealing kinetics: I. Experimental results. American Mineralogist, 84, 1213-1223

Chew, D.M., Petrus, J.A., and Kamber, B.S. (2014) U-Pb LA-ICPMS dating using accessory mineral standards with variable common Pb. Chemical Geology, 363, 185-199.

Crowley, K.D., Cameron, M., and Schaefer, R.I. (1991) Experimental studies of annealing of etched fission tracks in fluorapatite. Geochimica et Cosmochimica Acta, 55, 1449-1465.

Dartyge, E., Duraud, J.P., Langevin, Y., and Maurette, M. (1981) New model of nuclear particle tracks in dielectric minerals. Physical Review B, 23, 5213-5229.

Dartyge, E., and Sigmund, P. (1985) Tracks of heavy ions in muscovite mica: Analysis of the rate of production of radiation defects. Physical Review B, 32, 5429-5431.

Donelick, R.A. (1991) Crystallographic orientation dependence of mean etchable fission track length in apatite: an empirical model and experimental observations. American Mineralogist, 76, 83-91.

--- (1993) A method of fission track analysis utilizing bulk chemical etching of apatite. Patent No. 5,267,274, U.S.A.

--- (1995) A method of fission track analysis utilizing bulk chemical etching of apatite. Patent No. 658,800, Australia.

Donelick, R.A., Roden, M.K., Moers, J.D., Carpenter, B.S., and Miller D.S. (1990) Etchable length reduction of induced fission tracks in apatite at room temperature (~23°C): crystallographic orientation effects and "initial" mean lengths. Nuclear Tracks and Radiation Measurements, 17, 261-265.

Donelick, R.A., Ketcham, R.A., and Carlson, W.D. (1999) Variability of apatite fission-track annealing kinetics: II. Crystallographic orientation effects. American Mineralogist, 84, 1224-1234.

Fleischer, R.L., Price, P.B., and Walker, R.M. (1965) Effects of temperature, pressure, and ionization on the formation and stability of fission tracks in minerals and glasses. Journal of Geophysical Research, 70, 1497-1502.

--- (1975) Nuclear tracks in solids. Principles and applications. University of California Press, Berkeley, pp. 604.

Fleischer, R.L., Woods, R.T., Hart, H.R. Jr., Price, P.B., and Short, N.M. (1974) Effect of shock on fission track dating of apatite and sphene crystals from the Hardhat and Sedan underground nuclear explosions. Journal of Geophysical Research, 79, 339-342.

Galbraith, R.F. (2002) Some remarks on fission-track observational biases and crystallographic orientation effects. American Mineralogist, 87, 991–995.

Galbraith, R.F., and Laslett, G.M. (1988) some calculations relevant to thermal annealing of fission tracks in apatite. Proceedings of the Royal Society of London A, 419, 305-321.

Galbraith, R.F., Laslett, G.M., Green, P.F., and Duddy, I.R. (1990) Apatite fission track analysis: geological thermal history analysis based on a three-dimensional random process of linear radiation damage. Philosophical Transactions of the Royal Society of London A, 332, 419-438.

Gleadow, A.J.W., and Duddy, I.R. (1981) A natural long-term track annealing experiment for apatite. Nuclear Tracks, 5, 169-174.

Gleadow, A.J.W., Duddy, I.R., and Lovering, J.F. (1983) Fission track analysis: a new tool for the evaluation of thermal histories and hydrocarbon potential. Australian Petroleum Exploration Association Journal, 23, 93-102.

Green, P.F., Duddy, I.R., Gleadow, A.J.W., Tingate, P.R., and Laslett, G.M. (1986) Thermal annealing of fission tracks in apatite. 1. A qualitative description. Chemical Geology (Isotope Geoscience Section), 59, 237-253.

Hejl, E. (1995) Evidence for unetchable gaps in apatite fission tracks. Chemical Geology (Isotope Geoscience Section), 122, 259-269.

Jaskierowicz, G., Dunlop, A., and Jonckheere, R. (2004) Track formation in fluorapatite irradiated with energetic cluster ions. Nuclear Instruments and Methods in Physics Research B, 222, 213-227.

Johnstone, S., Hourigan, J., and Gallagher, C. (2013) LA-ICP-MS depth profile analysis of apatite: Protocol and implications for (U-Th)/He thermochronometry. Geochimica et Cosmochimica Acta, 109,143-161.

Jonckheere, R. (2003) On the ratio of induced fission-track densities in a mineral and a co-irradiated muscovite external detector with reference to fission-track dating of minerals. Chemical Geology, 200, 41-58.

Jonckheere, R., Enkelmann, E., Min, M., Trautmann, C., and Ratschbacher, L. (2007) Confined fission tracks in ion-irradiated and step-etched prismatic sections of Durango apatite. Chemical Geology, 242, 202-217.

Jonckheere, R., Van den haute, P., and Ratschbacher, L. (2015) Standardless fission-track dating of the Durango apatite age standard. Chemical Geology, 417, 44–57.

Ketcham, R.A. (2003) Observations on the relationship between crystallographic orientation and biasing in apatite fission-track measurements. American Mineralogist, 88, 817–829.

--- (2005) Forward and inverse modeling of low-temperature thermochronometry data. Reviews in Mineralogy and Geochemistry, 58, 275-314.

Ketcham, R.A., Carter, A., Donelick, R.A., Barbarand, J., and Hurford, A.J. (2007) Improved measurement of fission-track annealing in apatite using c-axis projection. American Mineralogist, 92, 789-798.

Ketcham, R.A., Carter, A., and Hurford, A.J. (2015) Inter-laboratory comparison of fission track confined length and etch figure measurements in apatite. American Mineralogist, 100, 1452-1468.

Ketcham, R.A., Donelick, R.A., and Donelick, M.B. (2000) AFTSolve: A program for multi-kinetic modeling of apatite fission-track data. Geological Materials Research, 2(1), (electronic: 18 pages, 2 tables, 12 figures). Mineralogical Society of America, Washington, D.C.

Kimura, J.-I., Danhara, T., and Iwano, H. (2000) A preliminary report on trace element determinations in zircon and apatite crystals using Excimer Laser Ablation - Inductively Coupled Plasma Mass Spectrometry (ExLA-ICPMS). Fission Track Newsletter, 13, 11-20.

Kluth, P., Afra, B., Rodriguez, M.D., Lang, M., Trautmann, C., and Ewing, R.C. (2012) Morphology and annealing kinetics of ion tracks in minerals. EPJ Web of Conferences, 35, 0300/1-4.

Kohn, B.P., Belton, D.X., Brown, R.W., Gleadow, A.J.W., Green, P.F., and Lovering, J.F. (2003) Comment on: "Experimental evidence for the pressure dependence of fission track annealing in apatite" by A.S. Wendt et al. [Earth Planet. Sci. Lett. 201 (2002) 593-607]. Earth and Planetary Science Letters, 215, 299–306.

Lang, M., Devanathan, R., Toulemonde, M., and Trautmann, C. (2015) Advances in understanding of swift heavy-ion tracks in complex ceramics. Current Opinion in Solid State and Materials Science, 19, 39-48.

Laslett, G.M., Gleadow, A.J.W., and Duddy, I.R. (1984) The relationship between fission track length and track density in apatite. Nuclear Tracks, 9, 29-38.

Li, W.-X., Wang, L., Lang, M., Trautmann, C., and Ewing, R.C. (2011) Thermal annealing mechanisms of latent fission tracks: Apatite vs. zircon. Earth and Planetary Science Letters, 302, 227–235.

Li, W.-X., Lang, M., Gleadow, A.J.W., Zdorovets, M.V., and Ewing R.C. (2012) Thermal annealing of unetched fission tracks in apatite. Earth and Planetary Science Letters, 321-322, 121–127.

Li, W.-X., Kluth, P., Schauries, D., Rodriguez, M.D., Lang, M., Zhang, F., Zdorovets, M., Trautmann, C., and Ewing R.C. (2014) Effect of orientation on ion track formation in apatite and zircon. American Mineralogist, 99, 1127-1132.

Miro, S., Grebille, D., Chateigner, D., Pelloquin, D., Stoquert, J.-P., Grob, J.-J., Costantini, J.-M., and Studer, F. (2005) X-ray diffraction study of damage induced by swift heavy ion irradiation in fluorapatite. Nuclear Instruments and Methods in Physics Research B, 227, 306-318.

Morishita, T., Hattori, K.H., Terada, K., Matsumoto, T., Yamamoto, K., Takebe, M., Ishida, Y., Tamura, A., and Arai, S. (2008) Geochemistry of apatite-rich layers in the Finero phlogopite-peridotite massif (Italian Western Alps) and ion microprobe dating of apatite. Chemical Geology, 251, 99-111.

Paul, T.A., and Fitzgerald, P.G. (1992) Transmission electron microscopic investigation of fission tracks in fluorapatite. American Mineralogist, 77, 336-344.

Pellas, P., and Perron, C. (1984) Track formation models: a short review. Nuclear Instruments and Methods in Physics Research, 31, 387-393.

Schauries, D., Afra, B., Bierschenk, T., Lang, M., Rodriguez, M.D., Trautmann, C., Li, W.-X., Ewing, R.C., and Kluth, P. (2014) The shape of ion tracks in natural apatite. Nuclear Instruments and Methods in Physics Research B, 326, 117-120.

Schmidt, J.S., Lelarge, M.L.M.V., Conceicao, R.V., and Balzaretti, N.M. (2014) Experimental evidence regarding the pressure dependence of fission track annealing in apatite. Earth and Planetary Science Letters, 390, 1-7.

Soares, C.J., Guedes, S., Hadler, J.C., Mertz-Kraus, R., Zack, T., and Iunes, P.J. (2014) Novel calibration for LA-ICP-MS-based fission-track thermochronology. Physics and Chemistry of Minerals, 41, 65-73.

Villa, F., Grivet, M., Rebetez, M., Dubois, C., Chambaudet, A., Chevarier, A., Martin, P., Brossard, F., Blondiaux, G., Sauvage, T., and Toulemonde, M. (1999) Damage morphology of Kr ion tracks in apatite: dependence on dE/dx. Radiation Measurements, 31, 65-70.

Watt, S., and Durrani, S.A. (1985) Thermal stability of fission tracks in apatite and sphene: using confined track length measurements. Nuclear Tracks, 10, 349-357.

Watt, S., Green, P.F., and Durrani, S.A. (1984) Studies of annealing anisotropy of fission tracks in mineral apatite using track-in-track, TINT, length measurements. Nuclear Tracks, 8, 371-375.

Wauschkuhn, B., Jonckheere, R., and Ratschbacher, L. (2015a) The KTB apatite fission-track profiles: building on a firm foundation? Geochimica et Cosmochimica Acta, 167, 27-62.

Wauschkuhn, B., Jonckheere, R., and Ratschbacher, L. (2015b) Xe- and U-tracks in apatite and muscovite near the etching threshold. Nuclear Instruments and Methods in Physics Research B, 343, 146-152.

Young, E.J., Myers, A.T., Munson, E.L., and Conklin, N.M. (1969) Mineralogy and geochemistry of fluorapatite from Cerro de Mercado, Durango, Mexico. U.S. Geological Survey Professional Paper, 650, 84-93.

Figure captions

Figure 1. Published step-etch data for induced fission tracks in apatite etched in nitric acid; mean confined-track length plotted against etch strength S_E (concentration × etch time); (a) Laslett et al. (1984; 5 M); (b) Watt et al. (1984; 1.3 M); (c) Watt and Durrani (1985; 1.3 M); (d) Green et al. (1986; 5 M); (e) Crowley et al. (1991; 1.6 M); (f) Carlson et al. (1999; 5.5 M); (g) Jonckheere et al. (2007; 5.5M); (h) Jonckheere et al. (2007; 4.0M); (i) Barbarand et al. (2003; 5M); (j) Barbarand et al. (2003; 0.8M); (k) Tello et al. (2006; 1.3 M); (l) Moreira et al. (2010; 0.75M); (m) Moreira et al. (2010; 1.5M); (n) Moreira et al. (5.0M). Like colors indicate like concentrations. Measurement errors, where cited, are in general less than the symbol size. The shaded interval corresponds to conditions producing confined tracks that are considered "well etched" or "full length". The etch-strength scale along the horizontal axis is a convenience; it is not implied that is accounts for all the differences between the different etches used.

Figure 2. Length distributions of the fossil (green), induced (yellow), and fossil plus induced (orange) confined tracks in step-etched prism sections of Durango apatite (bin width: 0.5 µm). The dashed lines are fitted Gaussian distributions. Statistics: n: number of tracks; m (µm) and s (µm): mean and standard deviation of the track length distribution.

Figure 3. Lengths of fossil and induced confined fission tracks in step-etched prism sections of Durango apatite plotted against their orientation to the **c**-axis. Green: fossil tracks in the unannealed Durango apatite; yellow: induced tracks in the neutron-irradiated, pre-annealed sample; orange: fossil and induced tracks in neutron-irradiated, unannealed sample; dashed lines: fitted ellipses plotted in Cartesian co-ordinates.

Figure 4. Means (a) and standard deviations (b) of length distributions of fossil (green), induced (yellow), and fossil plus induced (orange) confined fission tracks in prism sections of Durango apatite, plotted against etch time. (c) Plot of the ***a***-*versus* ***c***-axis lengths of ellipses fitted to the track length-*versus*-orientation data (green: fossil tracks; yellow: induced tracks; orange: fossil plus induced tracks); the small white squares are predictions of the mixed trend based on the fossil- and induced-track length data. The dashed lines in (a) are *ad hoc* sigmoidal fits to the data $l_M = \alpha / (1+\exp((t_E - \gamma)/\beta)$, with α (µm), β (s), and γ (s) constants. The dashed lines in (b) are *ad hoc* second degree polynomials fitted to the data; the

dashed lines in (c) are the 1:1 (diagonal) and the ***a***- *versus* ***c***-axis relationship of Donelick et al. (1999). Except where error bars are shown, the errors are smaller than the symbols.

Figure 5. Frequency distributions of the length increments between consecutive etch steps of fossil (green), induced (yellow), and fossil plus induced (orange) confined tracks in prism sections of Durango apatite (bins: 0.25 µm). Statistics: n: number of tracks; m (µm) and s (µm): mean and standard deviation of the length-increment distribution.

Figure 6. Length increments of fossil (green), induced (yellow), and fossil plus induced (orange) confined fission tracks plotted against the angle of the fission track to the crystallographic **c**-axis.

Figure 7. Lengths of single confined tracks in Durango apatite (fossil: green, induced: yellow, fossil plus induced: orange) at consecutive etch steps plotted against one another. The solid lines are geometric mean regression lines; the dashed diagonal lines are 1:1 lines.

Figure 8. Lengths of single fossil and induced confined fission tracks in prism sections of Durango apatite at 60 s etching plotted against their lengths at 20 s (5.5 M HNO_3, 21 °C). The solid lines are geometric mean regression lines; the dashed diagonal lines are 1:1.

Tables

Table 1. Confined track-length data

t_E (s)	N_C	L_M(1σ) (μm)	S_M(μm)	L_{MR}(1σ)(μm)	S_{MR}(1σ)(μm)	r	L_C(1σ) (μm)	L_A(1σ)(μm)	L_A/L_C(1σ)
				Fossil tracks					
20	298	14.47(05)	0.86	14.41(03)	0.83(03)	0.990	15.1(1)	14.2(1)	0.94(1)
30	253	14.97(05)	0.87	14.92(04)	0.91(04)	0.982	15.8(1)	14.6(1)	0.92(1)
40	226	15.49(06)	0.93	15.48(01)	0.90(01)	0.997	16.5(2)	15.1(1)	0.92(1)
50	191	15.82(07)	0.98	15.82(03)	0.89(03)	0.991	17.0(2)	15.4(1)	0.91(1)
60	172	16.21(08)	1.06	16.23(05)	1.00(05)	0.969	17.6(2)	15.7(1)	0.89(1)
				Induced tracks					
20	282	15.67(06)	0.93	15.71(01)	0.93(01)	0.998	15.7(1)	15.7(1)	1.00(1)
30	232	16.60(05)	0.81	16.57(02)	0.76(02)	0.994	16.7(1)	16.6(1)	0.99(1)
40	173	17.28(06)	0.80	17.27(01)	0.80(01)	0.996	17.5(2)	17.2(1)	0.98(1)
50	147	17.67(07)	0.84	17.67(04)	0.75(04)	0.973	17.9(2)	17.6(1)	0.98(1)
60	121	17.92(08)	0.88	17.87(04)	0.92(04)	0.978	18.2(2)	17.8(1)	0.98(1)
				Induced + fossil tracks					
20	205	15.63(08)	1.17	15.81(04)	1.15(04)	0.984	15.9(2)	15.5(1)	0.97(1)
30	181	16.47(08)	1.09	16.65(02)	0.97(02)	0.994	16.9(2)	16.3(1)	0.96(1)
40	141	16.96(09)	1.10	17.07(04)	1.06(04)	0.981	17.3(2)	16.8(1)	0.97(1)
50	107	17.25(10)	1.06	17.37(04)	1.06(04)	0.988	17.6(3)	17.1(2)	0.97(2)
60	75	17.55(12)	1.07	17.74(03)	0.90(03)	0.989	18.3(3)	17.3(2)	0.95(2)

t_E : etch time (5.5 M HNO_3, 21 °C); N_C: number of measured confined tracks; L_M(1σ): mean track length with 1σ statistical error; S_M: standard deviation of the mean; L_{MR}(1σ) and S_{MR}(1σ): mean and standard deviation of Gaussian distributions fitted to the track-length data; r: correlation coefficient of the regression; L_C(1σ) and L_A(1σ): major and minor axis of ellipses fitted to the track length-*versus*-orientation (angle to the **c**-axis) data.

Table 2. Properties of the sample with fossil and induced tracks

t_E (s)	L_{MS}/L_{MI}(1σ)	N_S/N_I(1σ)	L_C*(1σ)(μm)	L_A*(1σ)(μm)
20	0.92(01)	11.8(1)	15.6(7)	15.4(7)
30	0.90(01)	9.1(1)	16.5(7)	16.2(7)
40	0.90(01)	9.1(1)	17.3(8)	16.8(7)
50	0.90(01)	9.3(1)	17.7(8)	17.2(8)
60	0.90(01)	10.3(1)	18.0(8)	17.4(8)

L_{MS}/L_{MI}: ratio of fossil and induced mean track lengths; N_S/N_I: ratio of fossil and induced volumetric track densities; L_C* and L_A*: predicted major and minor-axis of ellipses fitted to the length-*versus*-orientation data.

Table 3. Confined track-length increments

Δt_E (s)	N_C	ΔL_M(1σ) (μm)	S_D (μm)
Fossil tracks			
20-30	253	0.49(02)	0.39
30-40	226	0.53(02)	0.33
40-50	191	0.40(02)	0.25
50-60	172	0.39(02)	0.24
20-60	172	1.69(04)	0.52
Induced tracks			
20-30	231	0.90(04)	0.61
30-40	172	0.64(03)	0.35
40-50	142	0.42(03)	0.38
50-60	119	0.28(03)	0.35
20-60	119	2.22(07)	0.81
Induced + fossil tracks			
20-30	179	0.84(04)	0.52
30-40	141	0.44(02)	0.29
40-50	106	0.34(02)	0.22
50-60	75	0.37(03)	0.23
20-60	75	1.99(08)	0.68

Δt_E: etch-time interval (5.5 M HNO_3, 21°C); N_C: number of measured track-length increments; ΔL_M(1σ): mean increment and 1σ error; S_D (μm): standard deviation of the track-length-increment distribution.

Figure 1

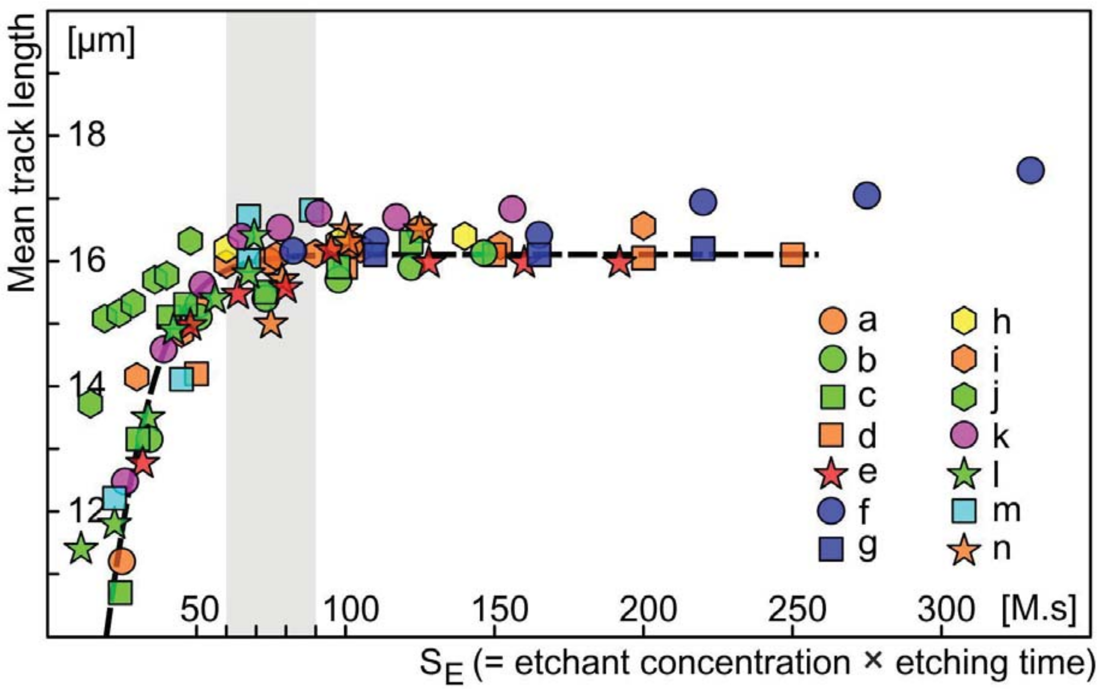
Mean track length
[μm]
18
16
14
12
50
100
150
200
250
300
[M.s]
S_E (= etchant concentration × etching time)
a
b
c
d
e
f
g
h
i
j
k
l
m
n

Figure 2

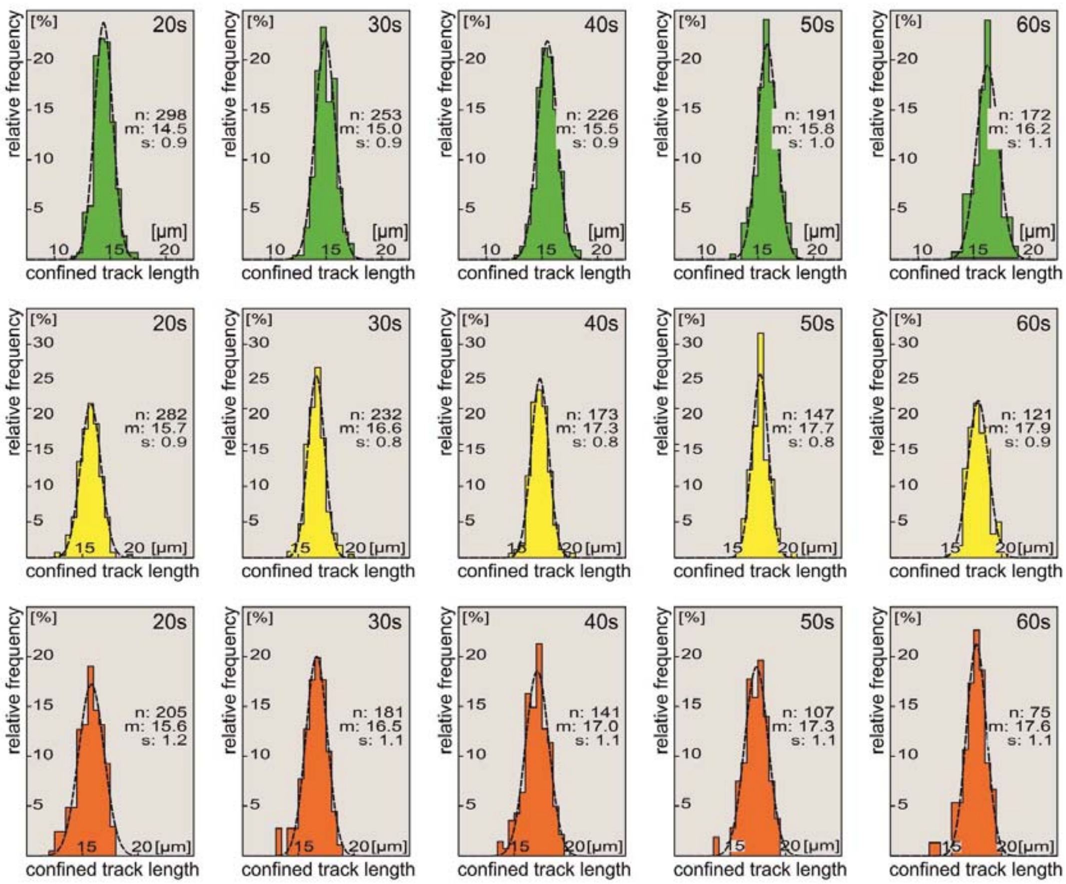
relative frequency
[%]
confined track length
[μm]
20s
n: 298
m: 14.5
s: 0.9
30s
n: 253
m: 15.0
s: 0.9
40s
n: 226
m: 15.5
s: 0.9
50s
n: 191
m: 15.8
s: 1.0
60s
n: 172
m: 16.2
s: 1.1
20s
n: 282
m: 15.7
s: 0.9
30s
n: 232
m: 16.6
s: 0.8
40s
n: 173
m: 17.3
s: 0.8
50s
n: 147
m: 17.7
s: 0.8
60s
n: 121
m: 17.9
s: 0.9
20s
n: 205
m: 15.6
s: 1.2
30s
n: 181
m: 16.5
s: 1.1
40s
n: 141
m: 17.0
s: 1.1
50s
n: 107
m: 17.3
s: 1.1
60s
n: 75
m: 17.6
s: 1.1

Figure 3

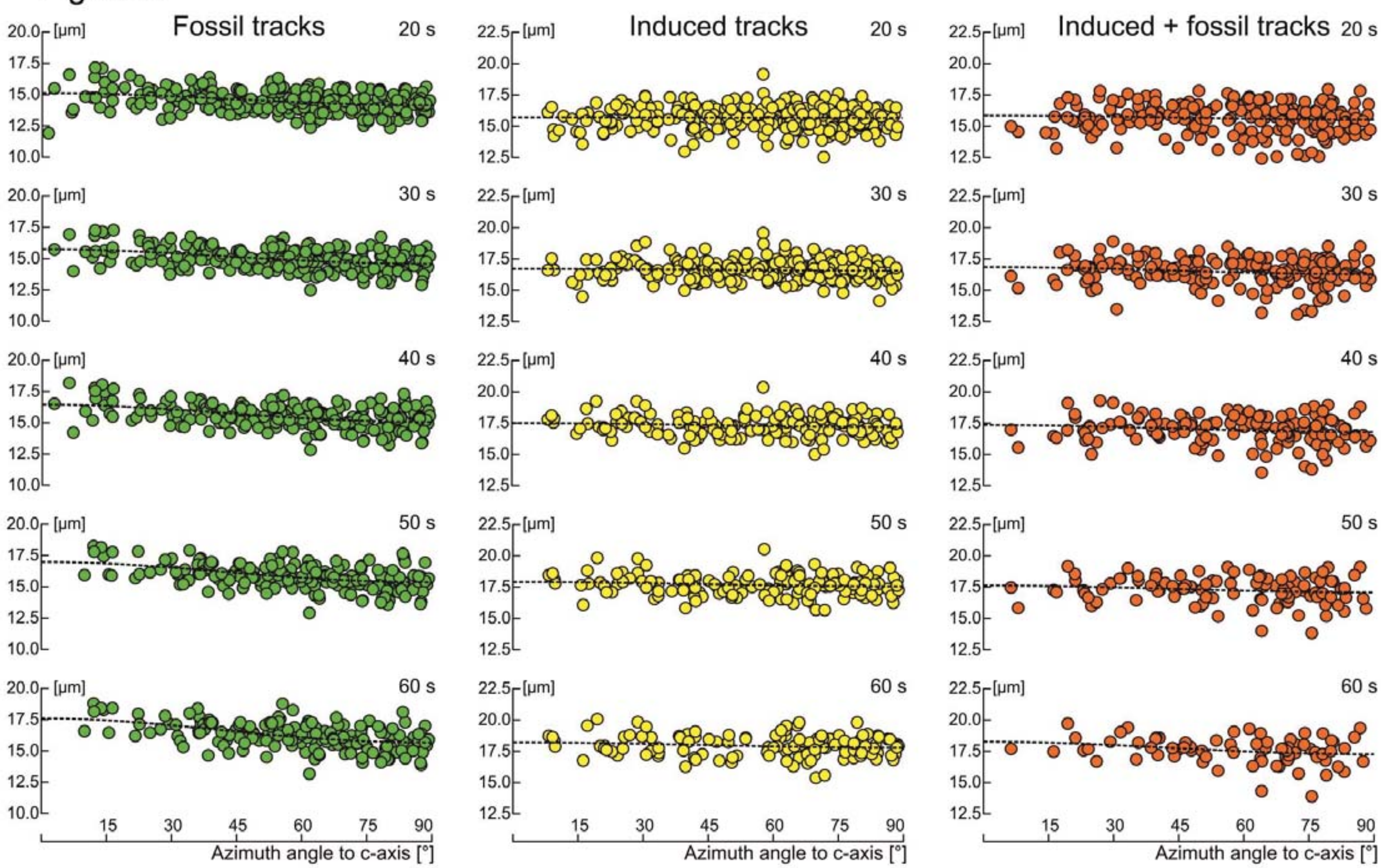
Fossil tracks
Induced tracks
Induced + fossil tracks
20 s
30 s
40 s
50 s
60 s
[µm]
20.0
17.5
15.0
12.5
10.0
22.5
15
30
45
60
75
90
Azimuth angle to c-axis [°]

Figure 4

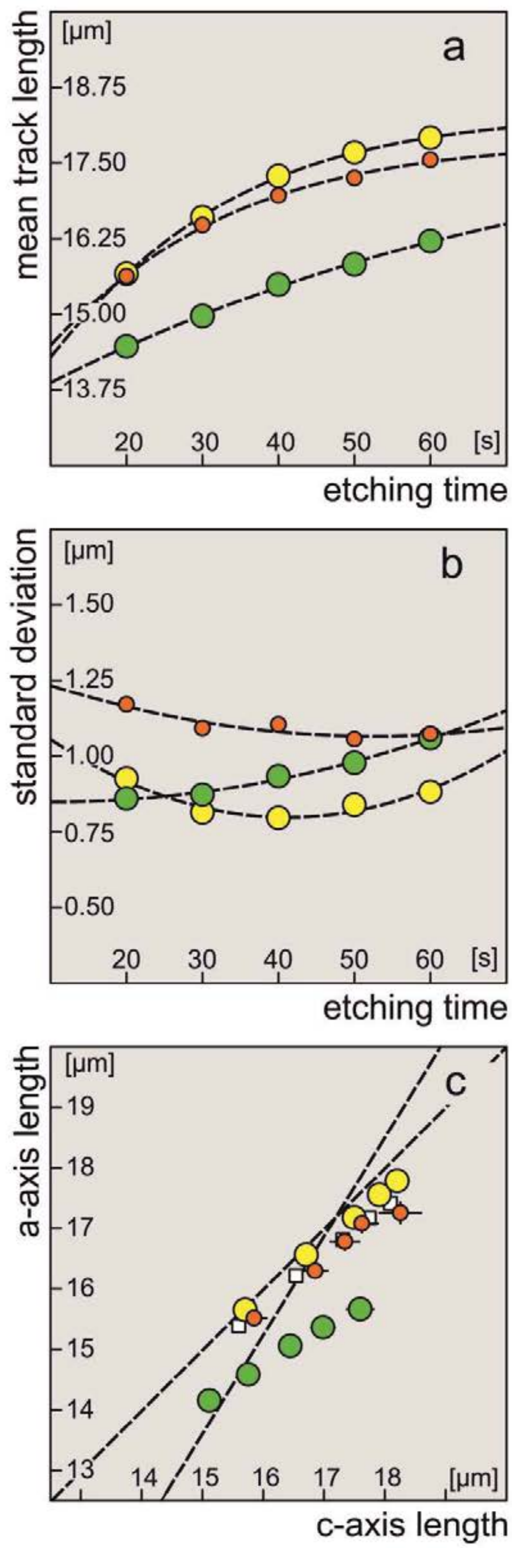
a
mean track length
[μm]
18.75
17.50
16.25
15.00
13.75
20
30
40
50
60
[s]
etching time
b
standard deviation
[μm]
1.50
1.25
1.00
0.75
0.50
20
30
40
50
60
[s]
etching time
c
a-axis length
[μm]
19
18
17
16
15
14
13
14
15
16
17
18
[μm]
c-axis length

This is a preprint, the final version is subject to change, of the American Mineralogist (MSA)
Cite as Authors (Year) Title. American Mineralogist, in press.
(DOI will not work until issue is live.) DOI: http://dx.doi.org/10.2138/am-2017-5988

Figure 5

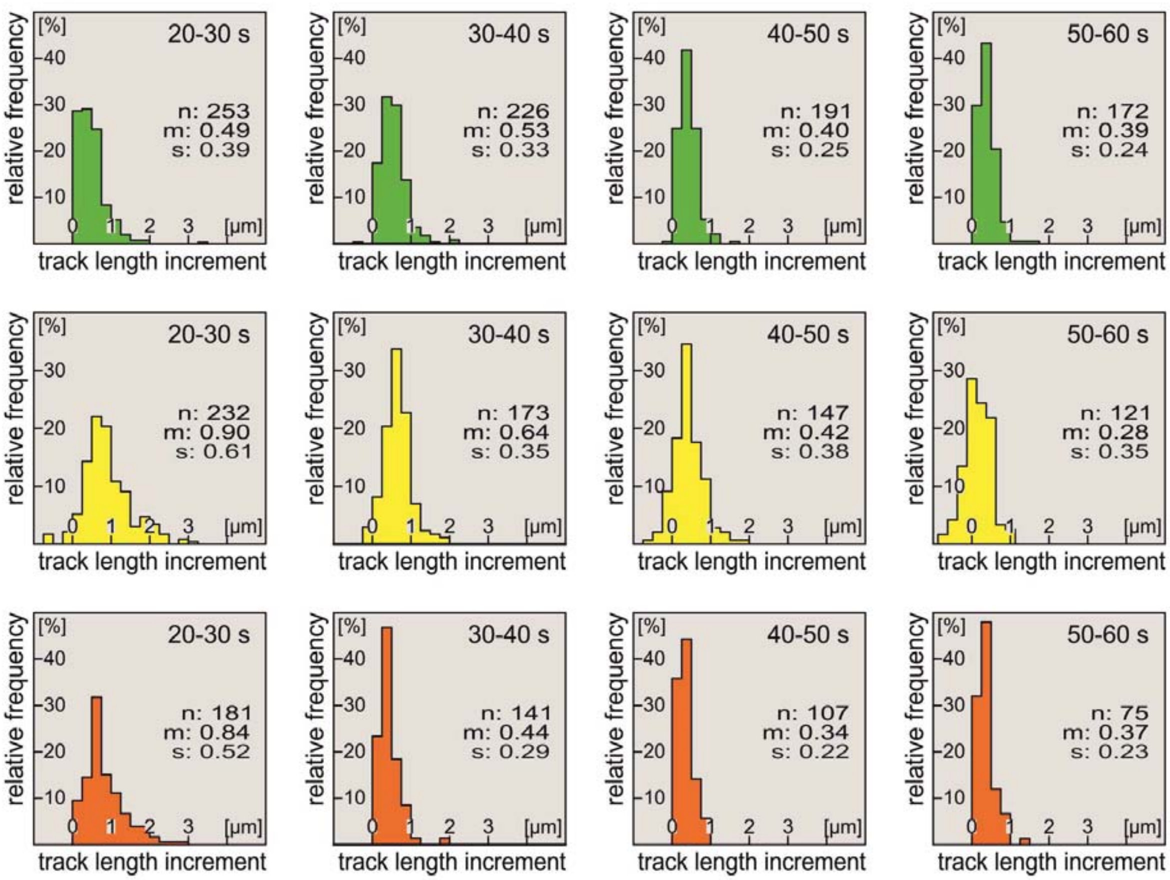

Figure 6

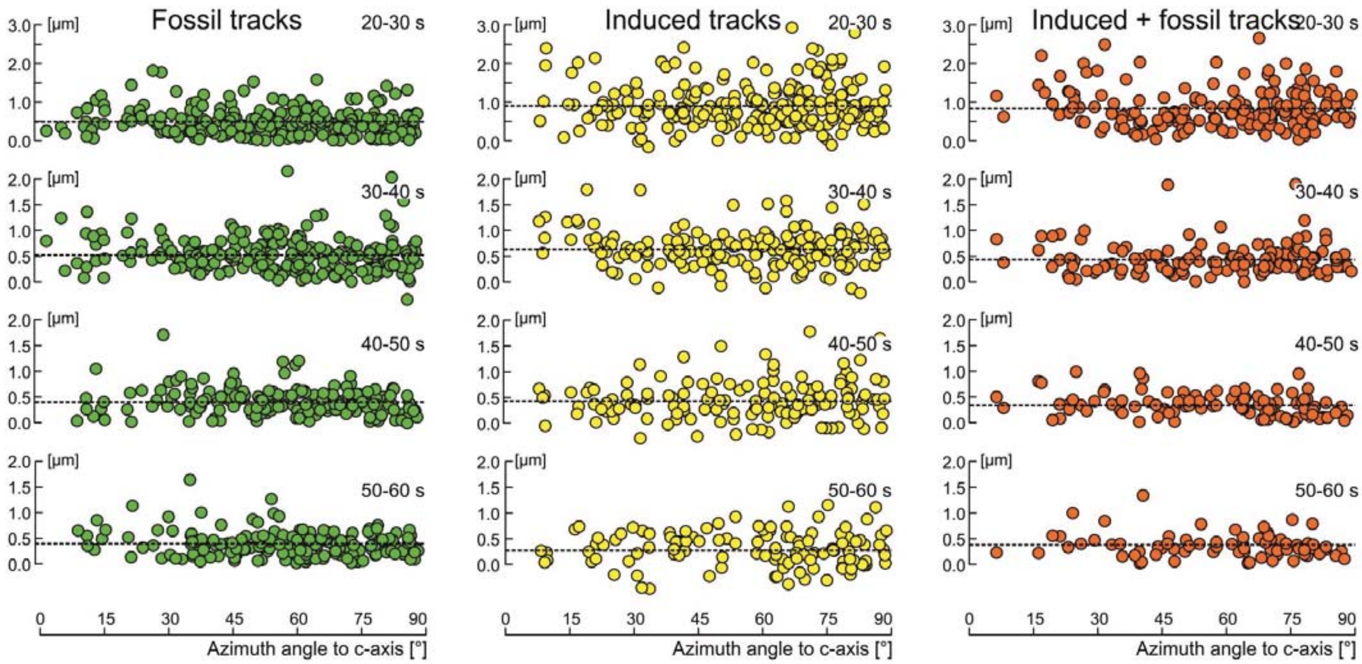
Fossil tracks
Induced tracks
Induced + fossil tracks
20-30 s
30-40 s
40-50 s
50-60 s
[µm]
Azimuth angle to c-axis [°]

Figure 7

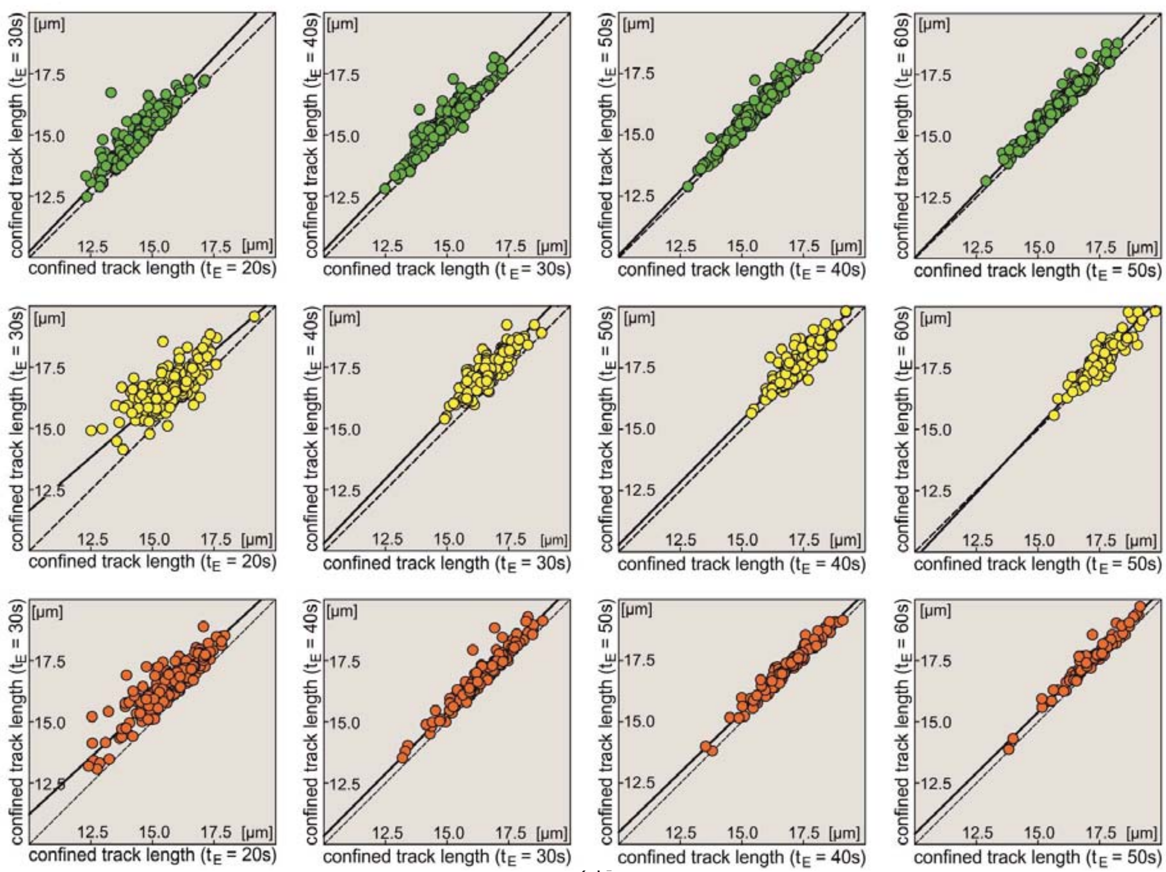
[μm]
17.5
15.0
12.5
12.5 15.0 17.5 [μm]
confined track length (t_E = 30s)
confined track length (t_E = 20s)
confined track length (t_E = 40s)
confined track length (t_E = 30s)
confined track length (t_E = 50s)
confined track length (t_E = 40s)
confined track length (t_E = 60s)
confined track length (t_E = 50s)

Figure 8

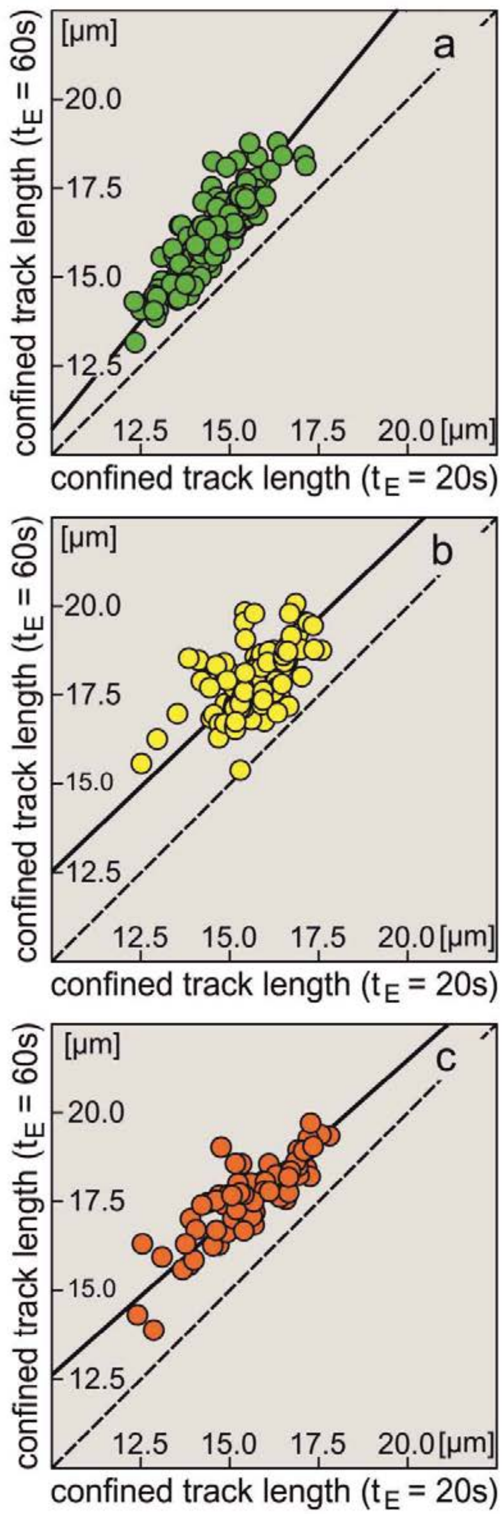
a
b
c
[µm]
20.0
17.5
15.0
12.5
12.5 15.0 17.5 20.0 [µm]
confined track length (t_E = 60s)
confined track length (t_E = 20s)